Journal of Nanobiotechnology

RESEARCH

Open Access

ROS-responsive nanoparticles for bioimaging and treating acute lung injury by releasing dexamethasone and improving alveolar macrophage homeostasis

Wenna Fan[1,2†], Yongyao Tang[2†], Yamin Liu[3†], Ya Ran[2,4†], Guangrui Pan[5†], Xin Song[2†], Li Mai[6], Xue Jiang[2], Dan Chen[2], Fangzhou Song[2*] and Haiyu Li[1*]

Abstract

Background Acute lung injury (ALI) triggers the activation of pulmonary macrophages, which in turn produce excessive amounts of reactive oxygen species (ROS).

Results We synthesized ROS-responsive red light-emitting carbon dots (RCMNs) that target lung macrophages, possess bioimaging capabilities, and efficiently eliminate intracellular ROS, thereby demonstrating anti-inflammatory effects for treating acute lung injury (ALI). In an LPS-induced ALI mouse model, RCMNs showed bioimaging and therapeutic potential, reducing lung damage and inflammation by targeting ROS-damaged tissue. RCMNs also improved alveolar macrophage activity, decreased inflammatory cytokines (TNF-α and IL-6), and enhanced survival in endotoxic shock, indicating their therapeutic potential for ALI. RNA-seq analysis revealed that RCMNs modulate signaling pathways related to calcium, TNF, and Toll-like receptors, highlighting their role in regulating inflammation and immune responses. Mechanistically, RCMNs alleviate inflammation in ALI by enhancing mitochondrial function in lung macrophages, as evidenced by improved mitochondrial morphology and membrane potential.

Conclusions This protective effect is mediated through the regulation of intracellular Ca^{2+} levels and mitochondrial respiratory chain complexes, suggesting RCMNs as a therapeutic strategy for mitochondrial dysfunction in ALI.

Keywords Acute lung injury, RCMNs nanoparticle, Alveolar macrophages, Mitochondrial function

†Wenna Fan, Yongyao Tang, Yamin Liu, Ya Ran, Guangrui Pan and Xin Song have authors contributed equally.

*Correspondence:
Fangzhou Song
fzsong@cqmu.edu.cn
Haiyu Li
lihaiyu@cqmu.edu.cn
Full list of author information is available at the end of the article

Graphical Abstract

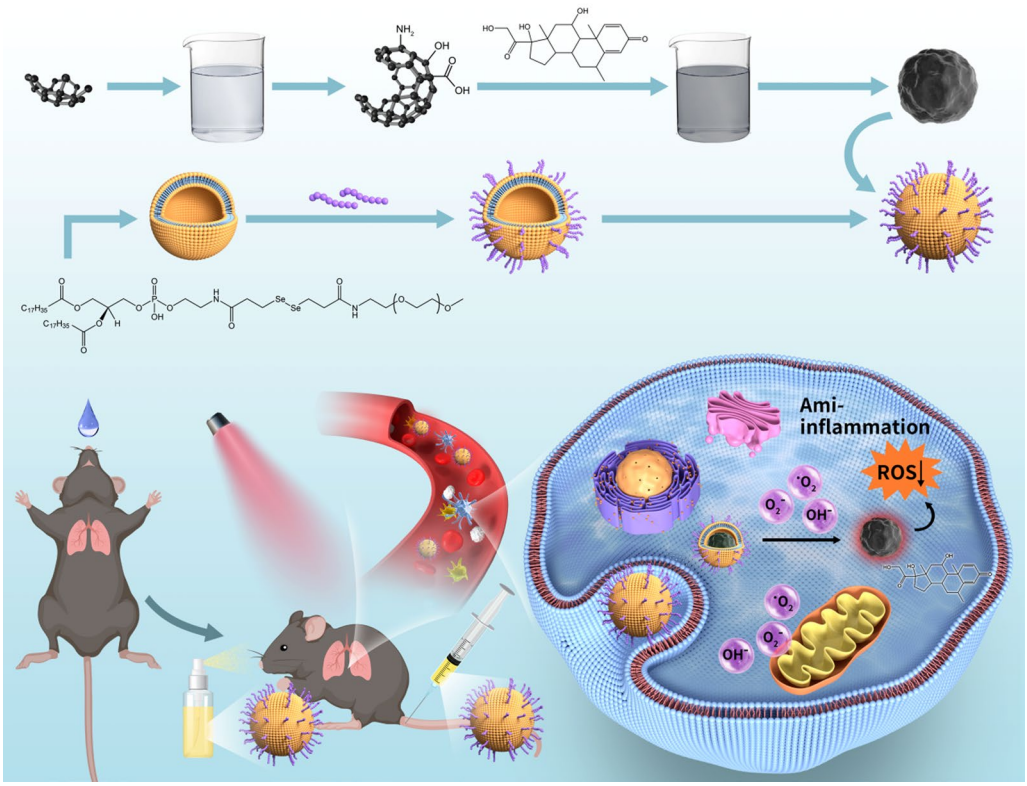

Introduction

Acute lung injury (ALI) is a severe clinical syndrome characterized by pulmonary inflammation, edema, and disruption of the alveolar capillary barrier. This disease can lead to respiratory dysfunction, and may even lead to multiple organ dysfunction and death [1–5]. Although there has been some progress in research on acute lung injury in the past few decades, its specific pathogenesis has not been fully elucidated. Macrophages, as the main immune cells in the lungs, play a crucial role in the pathogenesis of acute lung injury. Macrophages can not only eliminate pathogens and necrotic cells through phagocytosis, but also secrete various cytokines and inflammatory mediators, participating in regulating lung inflammatory response [4, 6–9]. However, in the case of acute lung injury, the response of macrophages is often too strong, leading to uncontrolled inflammatory response and worsening of lung injury.

In recent years, an increasing number of studies have shown that mitochondrial dysfunction of macrophages plays a crucial role in acute lung injury. Mitochondria are important organelles within cells, responsible for generating energy, synthesizing key molecules, and regulating processes such as cell death. In acute lung injury, mitochondrial dysfunction of macrophages can lead to excessive production of reactive oxygen species (ROS). These ROS not only directly cause cell damage, but also trigger and amplify inflammatory responses, exacerbating lung injury [10–13].The mechanism of action of ROS in acute lung injury includes disruption of the alveolar capillary barrier, activation of inflammatory cells, and degradation of extracellular matrix. In addition, ROS can induce macrophage polarization towards a pro-inflammatory phenotype, further exacerbating the inflammatory response [14–16]. Therefore, ROS produced by mitochondrial dysfunction of macrophages plays an important role in promoting acute lung injury. The development of multifunctional nanoparticles targeting macrophage mitochondria for ROS scavenging and anti-inflammatory therapy will be a promising strategy for treating ALI [17–19].

In this study, ROS responsive red light carbon dots TK-methylprednisolone nanoparticles (RCMNs) targeting macrophages were synthesized by adding NH2-TK

methylprednisolone to the carbon dots after EDC and NHS reactions, upon reaction, followed by DSPE-PEG-YEQDPWGVKWWY treatment via ultrasound and liposome extruder. The responsiveness of coordination bonds, formed between drug molecules and red carbon dots, ensures limited drug leakage under normal physiological conditions. However, within the high ROS level microenvironment of ALI, these bonds facilitate the rapid decomposition and release of drugs. To optimize targeting and prolong blood circulation, the nanoparticles are encapsulated within liposomes and equipped with macrophage-targeting peptides. Following systemic administration in ALI models, RCMN nanoparticles are primarily attracted to alveolar macrophages, leading to the prompt release of methylprednisolone and red light carbon dots. The RCMN nanoparticles represent a novel platform for activating immune homeostatic patterns of anti-inflammatory responses, thereby paving the way for improved efficacy of combination therapies.

Materials and methods

Synthesis of RCMNs

ROS-responsive red fluorescent carbon dot-TK-methylprednisolone nanoparticles (RCMNs) were successfully generated through a series of chemical reactions and purification steps. In brief, 30 mg of red fluorescent carbon dots were reacted with 1-Ethyl-3-(3'-dimethylaminopropyl)-carbodiimide(EDC) and N-hydroxysuccinimide (NHS) for 3 h, followed by an overnight reaction with NH2-TK-methylprednisolone. Subsequently, the mixture was dialyzed using a 1KD dialysis bag for 24 h to yield a pure product. Soybean phosphatidylcholine (SPC), cholesterol, DSPE-TK-PEG2K, and DSPE-PEG-YEQDPWGVKWWY were dissolved in 3 mL of chloroform. The solution was then reduced in a vacuum and evaporated to form a membrane within a sample bottle. This membrane was then immersed in the previously prepared red fluorescent carbon dot-TK-methylprednisolone complex and reconstituted with deionized water to a volume of 2 mL. To generate stable liposomes, the mixture was processed using ultrasound and a lipid extruder equipped with a polycarbonate membrane of 100 nm pore size. For further purification, the liposomes were dialyzed using a nanofiltration device equipped with a polycarbonate membrane of 30 nm pore size to remove any unencapsulated drug. Finally, the liposomes were reconstituted with deionized water to a volume of 10 mL. To maintain the stability of the liposomes, a cryoprotectant was added during the freeze-drying process. The preparation of red fluorescent carbon dot-TK-methylprednisolone liposomes offers a unique opportunity to investigate their biodistribution and pharmacokinetics in *vivo*. These liposomes are stable in suspension and can be easily administered intravenously for further evaluation in ALI models.

Characterization of RCMNs

The comprehensive evaluation of the synthesized RCMN nanomaterials has been conducted, utilizing multiple characterization methods. The morphology, particle size, and possible aggregation states of the RCMN were observed through transmission electron microscopy (TEM). The absorption spectra of the RCMN nanomaterials were accurately measured over specific wavelength ranges via ultraviolet–visible spectroscopy (UV–Vis). Through the analysis of these absorption spectra, the chemical composition of the RCMN, along with the properties of specific chemical bonds or functional groups present, could be determined. Additionally, the emission spectra of the RCMN under specific wavelength excitation were detected using a fluorescence spectrometer (FluoroMax-4). The particle size distribution, average particle size, and Zeta potential of the RCMN nanomaterials were measured via dynamic light scattering (DLS). To gain insight into the fluorescent behavior of the RCMN nanomaterials after interacting with cells, confocal laser scanning microscopy (CLSM) was employed for in-depth observations. To assess the imaging capabilities of the RCMN nanomaterials in an ALI mouse model, small animal live imaging equipment was utilized for imaging detection. By observing the distribution and changes in fluorescent signals in the mice, the potential of the RCMNs as a bioimaging agent for detecting ROS could be evaluated, thus exploring its potential application value in ALI models.

Experimental animal

Wild type C57BL/6 male mice aged 8–10 weeks (weighing 20-25 g) were purchased from the Experimental Animal Center of Chongqing Medical University. The mice were placed in a pathogen free environment with constant temperature (22 ± 2 ℃), constant humidity (50% ± 10%), and a 12 h light dark cycle, and given standard feed and drinking water. This research protocol has been approved by the Experimental Animal Management and Use Committee of Chongqing Medical University (Approval Number: IACUC-CQMU-2023-0289).

LPS induced ALI mouse model

6–8 weeks old C57BL/6 wild-type male were anesthetized by intraperitoneal injection of 2% pentobarbital sodium and subjected to non-invasive nebulization of LPS (2 mg/kg) using a laryngoscope and a microtracheal nebulizer. Immediately following administration, the mice's heads were positioned upright to facilitate the entry of the medication into the lungs for 1 min. The

establishment of an acute lung injury model has been proven successful when moist rales appear in the lungs of mice. Four hours post-injury, 10ug/kg RCMNs were administered via the tail vein or abdominal cavity. Subsequently, drug distribution was monitored every 4 h using a small animal live imaging device. Twenty-four hours after the acute injury, the mice were euthanized by inhalation of excess carbon dioxide, and blood and bronchoalveolar lavage fluid (BALF) were collected for analysis. The concentrations of inflammatory factors, including IL-1, IL-6, and IL-10 were detected using enzyme-linked immunosorbent assay (ELISA). The proportion changes of alveolar macrophages (anti CD11c, anti Siglec F) and macrophages (anti F4/80, anti CD11b) were identified by flow cytometry.

Lung histopathology

Mouse lung tissue was meticulously collected and fixed with 4% formaldehyde to ensure the preservation of its structural integrity and cellular morphology. After fixation, the tissue underwent a series of dehydration steps using graded alcohol solutions to effectively remove water and prepare the sample for embedding. Subsequently, the tissue was embedded in paraffin wax, facilitating the production of thin and uniform sections. These paraffin-embedded sections were then precisely cut using a microtome and mounted onto glass slides for further analysis. For histological examination, the sections were first deparaffinized and rehydrated through a series of alcohol solutions with decreasing concentrations. The sections were stained with Hematoxylin and Eosin (H&E) to enhance visualization of cellular and tissue structures under a light microscope.

Analysis of mitochondrial function using mitotracker fluorescent probes

MitoTracker Green is specific green fluorescent probe that selectively targets mitochondria, incorporating a carbocyanine fluorochrome. Its staining mechanism is independent of the mitochondrial membrane potential, enabling it to provide a thorough and unbiased depiction of the entire mitochondrial population within the cell. In contrast, MitoTracker Red accumulates within mitochondria in a manner that is contingent upon the membrane potential, functioning as a sensitive indicator for monitoring mitochondrial membrane potential dynamics. This probe is particularly advantageous for detecting cellular apoptosis by capturing alterations in membrane potential. Furthermore, MitoTracker Red, a red fluorescent dye, also exhibits accumulation in mitochondria driven by membrane potential. Upon oxidation within respiratory-active mitochondria, it fluoresces, serving as a marker for functionally intact mitochondrial subpopulations. In this study, we utilize flow cytometry to isolate a subpopulation of cells displaying a Green + / Red- staining profile. This staining pattern is indicative of compromised mitochondrial function, as evidenced by the absence of functional (Red-fluorescent) mitochondria despite the presence of the overall mitochondrial population (Green-fluorescent). MH-S cells were incubated with 100 nM of MitoTracker Green (Beyotime, China) for 30 min at 37 °C to quantify mitochondrial content. Subsequently, cells were treated with 50 nM of MitoTracker Red (Beyotime, China) for another 30 min at 37 °C to assess mitochondrial membrane potential. After incubation, cells were rinsed with pre-warmed staining buffer and analyzed using flow cytometry. The appropriate excitation and emission wavelengths for each fluorochrome were chosen in accordance with the manufacturer's guidelines.

MH-S cell treatment

MH-S mouse macrophages were procured from the Procell Life Science&Technology cell bank and were cultured in RPMI-1640 medium enriched with 10% fetal bovine serum. These macrophages were then incubated in a 37 ℃, 5% CO_2 incubator to facilitate their cultivation. After LPS stimulation (100 ng/mL) for 12 h, PBS, RCMNs, and dexamethasone were introduced for treatment.

ATP Measurement

Following the lysis of MH-S cells from various treatment groups, the resulting lysate was dispensed into white 96-well plates at a volume of 100 μL per well, in accordance with the established protocols. Subsequently, ATP levels were quantified using an ATP bioluminescent assay kit obtained from Beyotime Biotechnology (Shanghai, China), strictly following the manufacturer's recommended guidelines.

RNA-Seq and bioinformatics analysis

After acquiring RNA-Seq data derived from MH-S macrophages stimulated with RCMNs (1 μg/mL) in the presence of LPS (100 ng/mL), a comprehensive bioinformatics analysis was conducted to decipher the transcriptome profiles and pinpoint differentially expressed genes (DEGs). The raw bulk RNA-Seq data and processed datasets generated for this study have been concurrently deposited in the Gene Expression Omnibus (GEO) repository and can be accessed using the accession number GSE277635. Initially, the raw sequencing reads underwent meticulous quality control assessments utilizing tools such as FastQC, aimed at evaluating sequence quality metrics. These reads might have been subjected to preprocessing procedures, including

adapter trimming and filtering, to eliminate low-quality sequences. Subsequently, the refined reads were meticulously aligned to a reference genome, typically leveraging alignment algorithms like HISAT2. FeatureCounts was then employed to precisely quantify the abundance of reads mapped to each gene. Principal Component Analysis (PCA) was executed using the built-in R function prcomp` to reduce data dimensionality and visualize disparities between groups. Differential expression analysis between treatment groups was conducted utilizing the DESeq2 R package (version 1.26.0). Genes exhibiting an adjusted P-value < 0.05 and an absolute Log_2 Fold Change exceeding 1 (|Log2FC| > 1) were deemed as differentially expressed. To gain deeper insights into the biological implications of the identified DEGs, pathway analysis was conducted using the Cluster Profiler R package. The KEGG (Kyoto Encyclopedia of Genes and Genomes) pathway database served as a vital reference for annotating and categorizing genes into biologically relevant pathways. Amongst the DEGs, the ones with an adjusted P-value < 0.05 were further subjected to pathway analysis. The top significantly enriched pathways, based on statistical significance and pertinence to the experimental setup, were carefully selected for presentation, providing valuable insights into the underlying biological mechanisms.

Mouse mitochondrial energy metabolism PCR array

Total RNA was extracted from the samples using Trizol reagent (Thermo, USA), and 1 μg of the extracted RNA was then subjected to mRNA reverse transcription using the HiScriptII One Step RT-PCR Kit (TAKARA, Beijing, China) to generate total cDNA. Following the manufacturer's prescribed protocol, the gene expression profile was analyzed using mouse mitochondrial energy metabolism PCR array (Wcgene Biotech, Shanghai, China). To ensure precision, β-actin (ACTB) and glyceraldehyde 3-phosphate dehydrogenase (GAPDH) were selected as endogenous controls. The cDNA was then used in quantitative PCR reactions, which were performed in 96-well plates using the TB Green Premix (TAKARA, Beijing, China) on the CFX 96 (Bio-Rad, USA) under the following conditions: 95 °C for 5 min, 40 cles of 95 °C for 5 s, and 60 °C for 30 s. The mouse mitochondrial energy metabolism PCR array contains 90 genes and 4 endogenous reference genes. The quantitative expression levels were analyzed using the $2^{-\Delta\Delta Ct}$ method.

Flow cytometry detection of Ca^{2+} and ROS levels

MH-S cells were seeded in a confocal microscopy culture dish and incubated overnight under appropriate conditions to ensure cell fusion degree of 60%. This was followed by stimulating the cells with LPS for 6 h to mimic the inflammatory environment of acute lung injury. To assess the intracellular calcium ion concentration and ROS levels, fluorescent probes Fluo-3/AM (1 μM) and DCFH2-DA (1 μM) were used. These probes bind specifically to their target molecules, allowing for the detection of intracellular calcium ion concentration and ROS levels, respectively. After incubating with the cells for a certain period of time, the fluorescent probes bound to their target molecules. The specific excitation wavelength was used to excite the fluorescent probes and detect the fluorescence intensity. The collected data were processed and analyzed using computer software to quantitatively analyze the changes in Ca^{2+} and ROS levels.

Statistical analysis

The data were meticulously analyzed using Prism 8.0 (GraphPad, USA) software. When comparing two sets of data, the unpaired two-tailed Student's t-test was employed. Prior to the t-test, a test for variance similarity (F-test) was conducted to ensure that there were no significant differences in the variances of the two datasets, thereby fulfilling the prerequisite assumption of the t-test. In this study, $p < 0.05$ was considered to be statistically significant.

Results

Preparation and characterization of ROS responsive nanoparticles targeting acute lung injury

Previous research has established a strong association between acute lung injury (ALI) and uncontrolled reactive oxygen species (ROS), which play a crucial role in lung damage. Consequently, scavenging ROS is regarded as a promising therapeutic approach for these conditions. In acute lung injury, the abnormal activation of macrophages with mitochondrial dysfunction is closely linked to ROS production and significantly affects the progression of lung inflammation and injury [20]. In this study, we have carefully synthesized ROS-responsive red fluorescent carbon dot-TK-methylprednisolone nanoparticles (RCMNs) through a series of precisely controlled chemical reactions and rigorous purification steps, specifically tailored to target acute lung injury. The morphological features of RCMNs were characterized by transmission electron microscope (TEM, Fig. 1A), showing an average size of 78 ± 5.2 nm which matched the hydrodynamic diameter of 83 ± 4.8 nm measured by dynamic light scattering (DLS, Fig. 1B). The absorption bands located at 2924 and 3000 cm^{-1} correspond to the stretching vibrations of N–H and O–H, respectively (Fig. 1C). Meanwhile, the RCMNs particles exhibit a UV–Vis absorption wavelength of approximately 214 nm, as depicted in Figs. 1D. Furthermore, RCMNs demonstrated excellent

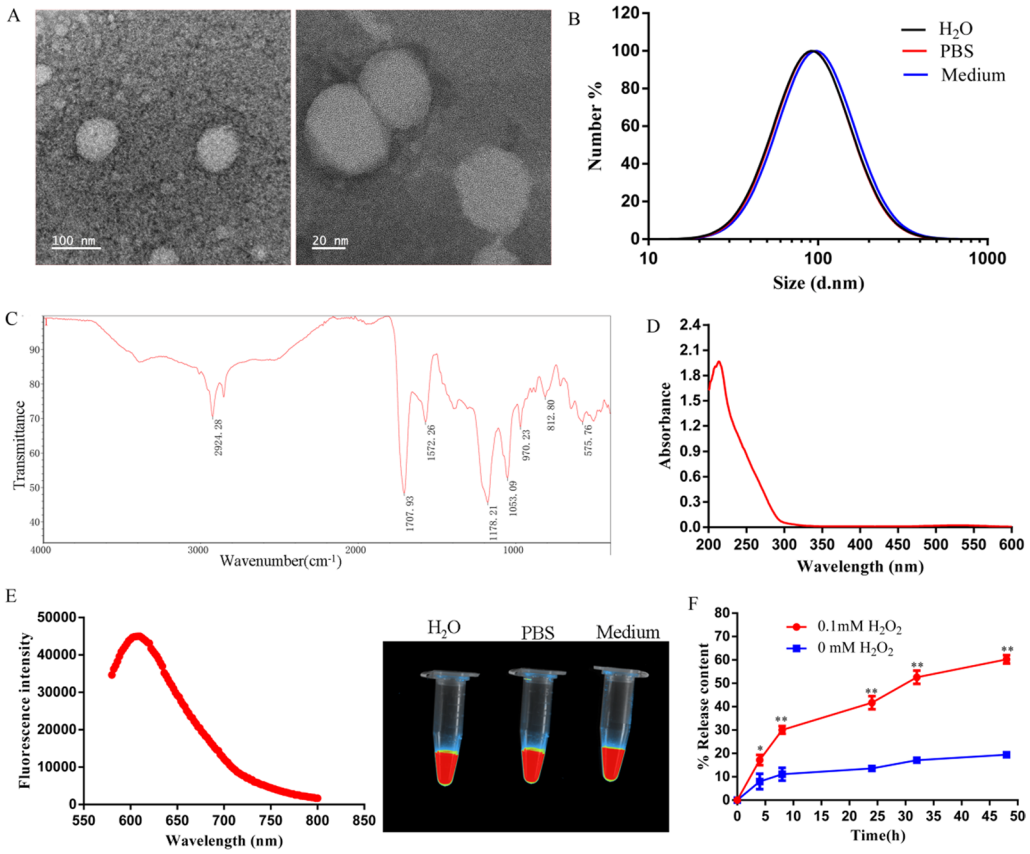

Fig. 1 Physical characterization of RCMNs. **A** The morphology of RCMNs was detected by TEM. **B** The hydrodynamic dimensions of RCMNs in different solutions were detected by DLS. **C** Detection of RCMNs using fourier transform infrared spectrometer. **D** UV spectra of RCMNs. **E** Fluorescence spectra of RCMNs and fluorescence detection of RCMNs in different solutions. **F** The cumulative release of RCMNs in H_2O_2 with different concentrations

solubility and stability in water, phosphate buffered saline (PBS), and cell culture medium, maintaining their properties for up to one week. Additional fluorescence spectroscopy analysis further revealed that RCMNs possess a red fluorescence excitation wavelength of 520 nm and an emission wavelength of 620 nm, exhibiting intense red fluorescence in all three solvents (Fig. 1E). To assess the drug release rate of RCMNs in response to ROS, cumulative release experiments were performed using varying concentrations of hydrogen peroxide (H_2O_2). As depicted in figure 1F, RCMNs remain largely inactive in the absence of 0 mM H_2O_2, releasing only approximately 17% of the drug over a 50-h incubation period. Notably, the presence of ROS triggers a rapid release of drugs from the RCMNs. Specifically, in the presence of 0.1 mM H_2O_2, the release rate increases significantly to 70% over the same 50-h period (Fig. 1F). These results indicate that the synthesized RCMNs can remain stable in the bloodstream to eliminate premature drug release, and can quickly expose loaded drugs targeting ROS and inflammation.

Bioimaging and therapeutic effects of RCMNs nanoparticles in LPS-Induced ALI mouse model

To investigate the efficacy of RCMNs in scavenging ROS and treating acute lung injury, an LPS-Induced ALI mouse model was constructed. Following intraperitoneal injection, the RCMNs are efficiently absorbed into the bloodstream through the peritoneal membrane and the omental vessels. The fluorescent properties of the RCMNs facilitate their detection and visualization within tissues, providing insights into their biodistribution and targeting efficiency. When comparing the distribution of RCMNs nanoparticles in healthy mice versus those with ALI, it was noticed that these RCMNs were significantly more concentrated in the lungs of ALI mice (Fig. 2A). This suggests that the RCMNs have an inherent ability to target sites of inflammation. To further investigate the pharmacokinetic behavior of RCMNs, their fluorescence was tracked in both healthy and ALI mice. Following injection, significant accumulation of RCMNs was observed in the liver and lungs. However, the rapid decrease in RCMN accumulation in healthy

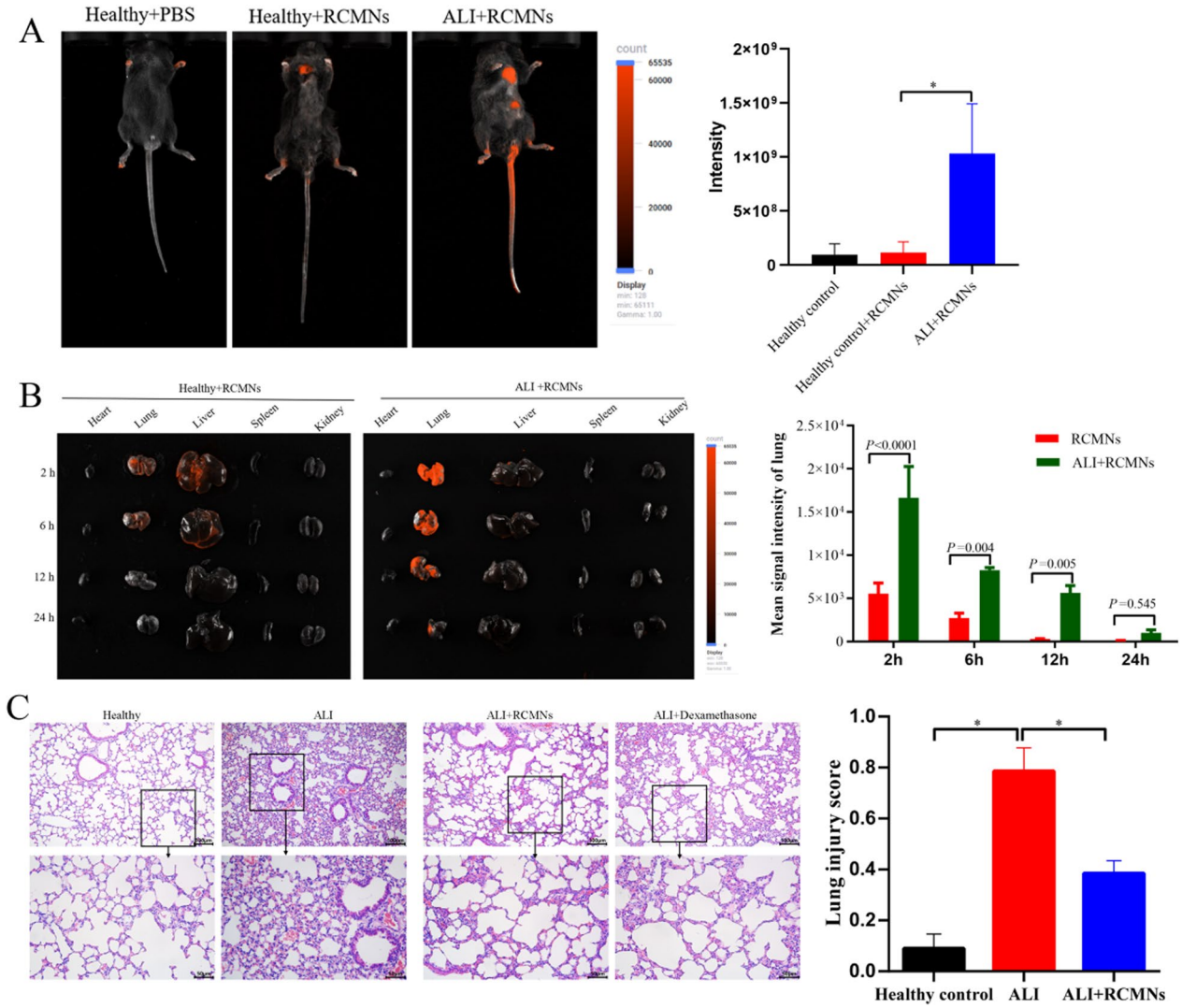

Fig. 2 Bioimaging and therapeutic effects of RCMNs in ALI mouse model. **A** The distribution of RCMNs was observed in *vivo* in both healthy and ALI mice following a 2 h injection, and statistics were collected on the intensity of red fluorescence in the mice. **B** The distribution of RCMNs in the primary organs of healthy and ALI mice was examined, along with a statistical analysis of the corresponding red fluorescence intensity. **C** The histological images depict H&E-stained lung sections, and the lung injury score was determined by evaluating five pathophysiological characteristics observed in these images. The scale bar represents 50 μm

mice indicated effective metabolism and clearance from the body. Importantly, higher accumulation of RCMNs was observed in the lungs of ALI mice compared to healthy mice (Fig. 2B), further demonstrating the ability of RCMNs to target ROS-damaged tissue. The therapeutic potential of RCMNs was comprehensively evaluated in an LPS-induced acute lung injury (ALI) mouse model, utilizing a dose of 10 mg/kg. To facilitate robust data comparison, dexamethasone was employed as a positive control. Twenty-four hours after the LPS challenge, lung tissue was harvested and stained with hematoxylin and eosin (H&E) to enable histological assessment of inflammatory cell infiltration. Notably, animals that received RCMNs exhibited significantly alleviated lung damage, evidenced by reduced inflammatory cell infiltration and thinning of the alveolar wall (Fig. 2C). These results suggest valuable insights into the potential of RCMNs as effective therapeutic agents for ALI.

Anti-inflammatory properties of RCMNs in LPS-induced ALI

Furthermore, we conducted a comprehensive evaluation of the anti-inflammatory effects of RCMNs in LPS-induced acute lung injury (ALI). Utilizing flow cytometry, the administration of RCMNs was found to significantly

increase the percentage of alveolar macrophages (AMs) in bronchoalveolar lavage fluid (BALF), which play a crucial role in maintaining tissue homeostasis and facilitating repair processes during ALI (Fig. 3A). Alveolar macrophages (AMs) can facilitate lung tissue repair during ALI. They secrete growth factors and other molecules

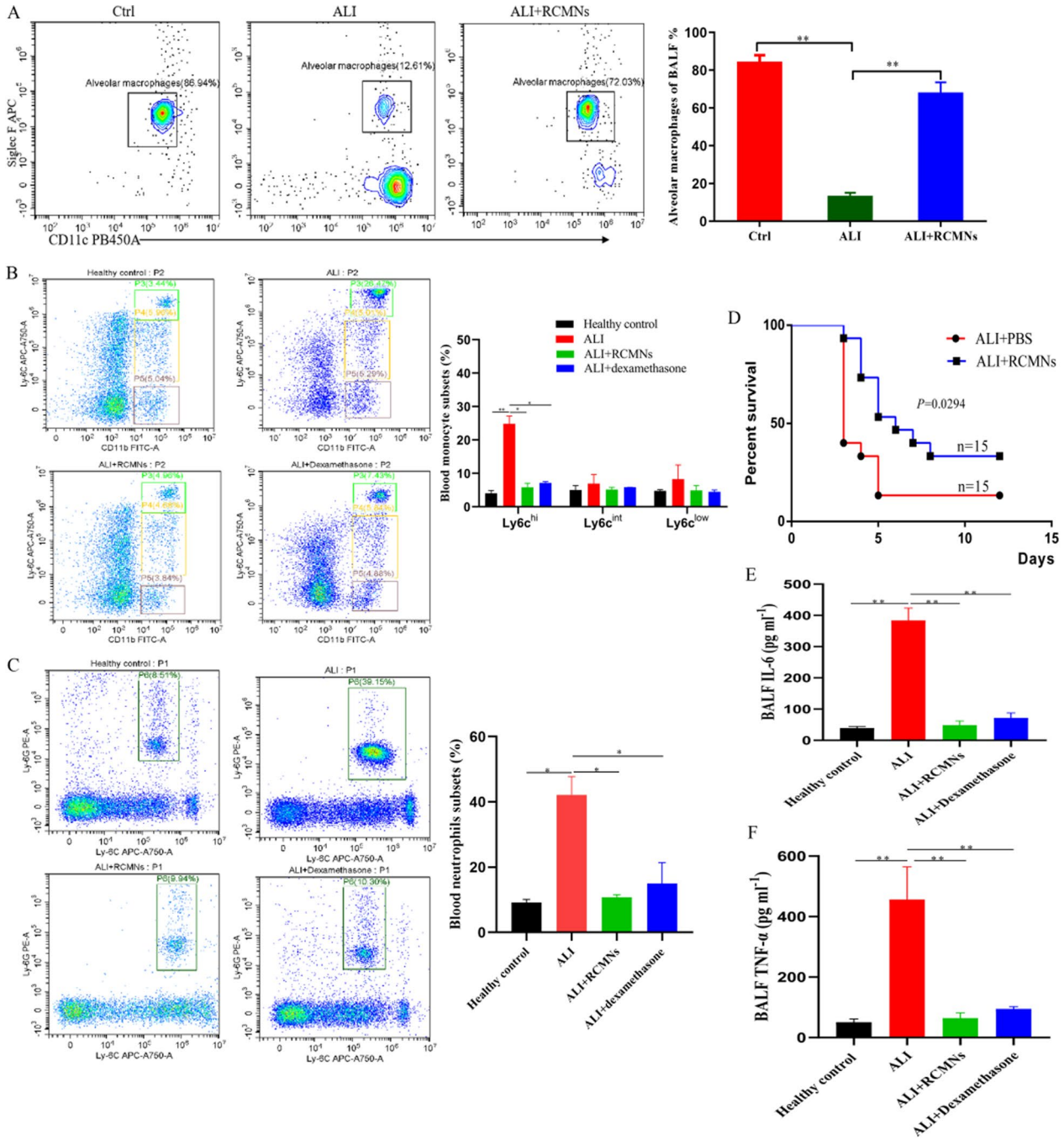

Fig. 3 Therapeutic effects of RCMNs in alleviating lung inflammation and injury in mice. **A** Flow cytometry analysis of bronchoalveolar lavage fluid (BALF) reveals the population of alveolar macrophages ($CD11c^{+}SiglecF^{+}$), identified by gating on $CD45^{+}SiglecF^{+}CD11c^{+}$ cells. **B** The proportion of classical monocytes ($CD45^{+}CD11b^{+}$ $Ly6C^{hi}$) in the blood was found to decrease following treatment with RCMNs (**C**) Flow cytometry analysis of blood neutrophils ($CD45^{+}CD11b^{+}$ $Ly6G^{+}$) shows a decrease in neutrophil counts in ALI mice receiving RCMNs. **D** Survival curves demonstrate a significant improvement in the survival rate of mice challenged with a high dose of LPS (10 mg/kg) and subsequently treated with RCMNs compared to the PBS control group. **E**, **F** Quantification of interleukin-6 (IL-6) and tumor necrosis factor (TNF) levels in BAL fluid

that promote the proliferation and migration of lung epithelial cells, which is crucial for restoring the integrity of the alveolar barrier. Conversely, a notable decrease in the presence of inflammatory $CD45^+CD11b^+$ $Ly6C^{high}$ monocytes and $CD45^+CD11b^+Ly6G^+$ neutrophils in the blood was observed following RCMN treatment (Fig. 3B, C). These findings are providing compelling evidence for the anti-inflammatory and tissue-protective properties of RCMNs in severe inflammatory lung disorders. To further validate these observations, the study also investigated the protective effects of RCMNs in a mice model of endotoxic shock. The administration of RCMNs led to a substantial improvement in the survival rate of mice exposed to a lethal dose of endotoxin (Fig. 3D). A key aspect of this study involved assessing the impact of RCMNs on biomarkers of acute inflammation, specifically tumor necrosis factor (TNF-α) and interleukin-6 (IL-6). The results indicated that RCMNs significantly reduced the levels of TNF-α and IL-6 in the bronchoalveolar lavage fluid (BALF) of mice with LPS-induced ALI (Fig. 3E, F).This finding provides further evidence for the anti-inflammatory properties of RCMNs and suggests their potential therapeutic benefits in modulating the inflammatory response in ALI.

RCMNs alleviate inflammation by regulating the metabolic homeostasis of macrophage mitochondria

Macrophage mitochondria are critical regulators in acute lung injury (ALI), influencing energy metabolism, oxidative stress responses, inflammatory signaling, and cell death pathways. Dysfunctional mitochondria within these immune cells can exacerbate lung tissue damage and hinder repair processes. We investigated the effects of RCMNs on mitochondrial morphology and function in primary macrophages isolated from mouse lungs following LPS stimulation. Our results showed that RCMNs effectively alleviated mitochondrial ROS stress and reduced the proportion of dysfunctional mitochondria in these cells, as evidenced by MitoRed/Green Tracker staining (Fig. 4A, B). Furthermore, TEM analysis revealed ultrastructural changes in mitochondria from LPS-challenged mice lung tissue, including a reduced number of mitochondria with disorganized cristae and vacuolar formations. However, in LPS-challenged mice treated with RCMNs, we observed an increase in mitochondrial number and improved mitochondrial morphology, along with enhanced mitochondrial membrane potential (Fig. 4C). These findings suggest that RCMNs alleviate mitochondrial ROS stress, reduce dysfunctional mitochondria, and improve mitochondrial morphology in primary macrophages from mouse lungs with acute lung injury, indicating their potential to mitigate lung tissue damage and promote repair processes.

Targeting specificity and ROS-scavenging capabilities of RCMNs on lung macrophages in vitro

To further validate the possibility of RCMNs specifically targeting mitochondrial components of macrophages, MH-S cells, a mouse alveolar macrophage cell line, were first incubated with 10ug/ml of RCMNs. Confocal laser scanning microscopy (CLSM) demonstrated that the red fluorescent RCMNs were internalized and co-localized with the mitochondria of MH-S cells labeled by Mito Tracker Green (Fig. 5A). As shown in Fig. 5B, the administration of RCMNs significantly reduced the apoptosis rate (AnV^+/PI^+) of MH-S cells induced by LPS. The application of RCMNs after LPS treatment alleviated mitochondrial ROS stress as detected by Mito Sox Green (Fig. 5C). Mitochondrial dysfunction during LPS-induced acute lung injury can lead to a decrease in ATP production, which is essential for cellular functions. This reduction in ATP may exacerbate cellular damage and inflammatory responses, highlighting the importance of mitochondrial integrity and ATP production in limiting the severity of LPS-induced lung injury. Furthermore, RCMNs promote ATP production and decrease the percentage of macrophages with dysfunctional mitochondria in LPS stimulated MH-S cells, as detected by MitoRed/Green Tracker stacking (Fig. 5D, E). These data demonstrate that RCMNs specifically target mitochondrial components of macrophages, reducing apoptosis, mitochondrial ROS stress, and dysfunction while promoting ATP production in LPS-induced acute lung injury in mouse alveolar macrophage cell line MH-S.

Identification of mitochondrial respiratory chain as anti-inflammatory mechanism of RCMNs

To reveal the molecular biological mechanism of RCMNs in the treatment of acute lung injury, MH-S cells were stimulated by LPS and treated with RCMNs followed by RNA-seq transcriptome analysis. Principal Component Analysis (PCA) validates previous observations indicating that, in response to LPS-induced ALI, RCMNs significantly alter their gene expression profile (Fig. 6A). Moreover, after 48 h of RCMNs treatment, there remains a notable difference between the ALI group and the RCMNs-treatment group, with the latter aligning closely with the control group (Fig. 6A). The differentially expressed genes ($\geq$ twofold absolute change from sea level baseline, $q < 0.05$) in the control group, LPS group and LPS + RCMNs group were shown in the volcano plot (Fig. 6B). The heatmap showed the top 80 differentially expressed genes in the control group, as well as in the LPS group and the LPS + RCMNs group (Fig. 6C). Functional enrichment analysis of the genes that exhibited significant differential expression following RCMNs treatment revealed their primary involvement in several

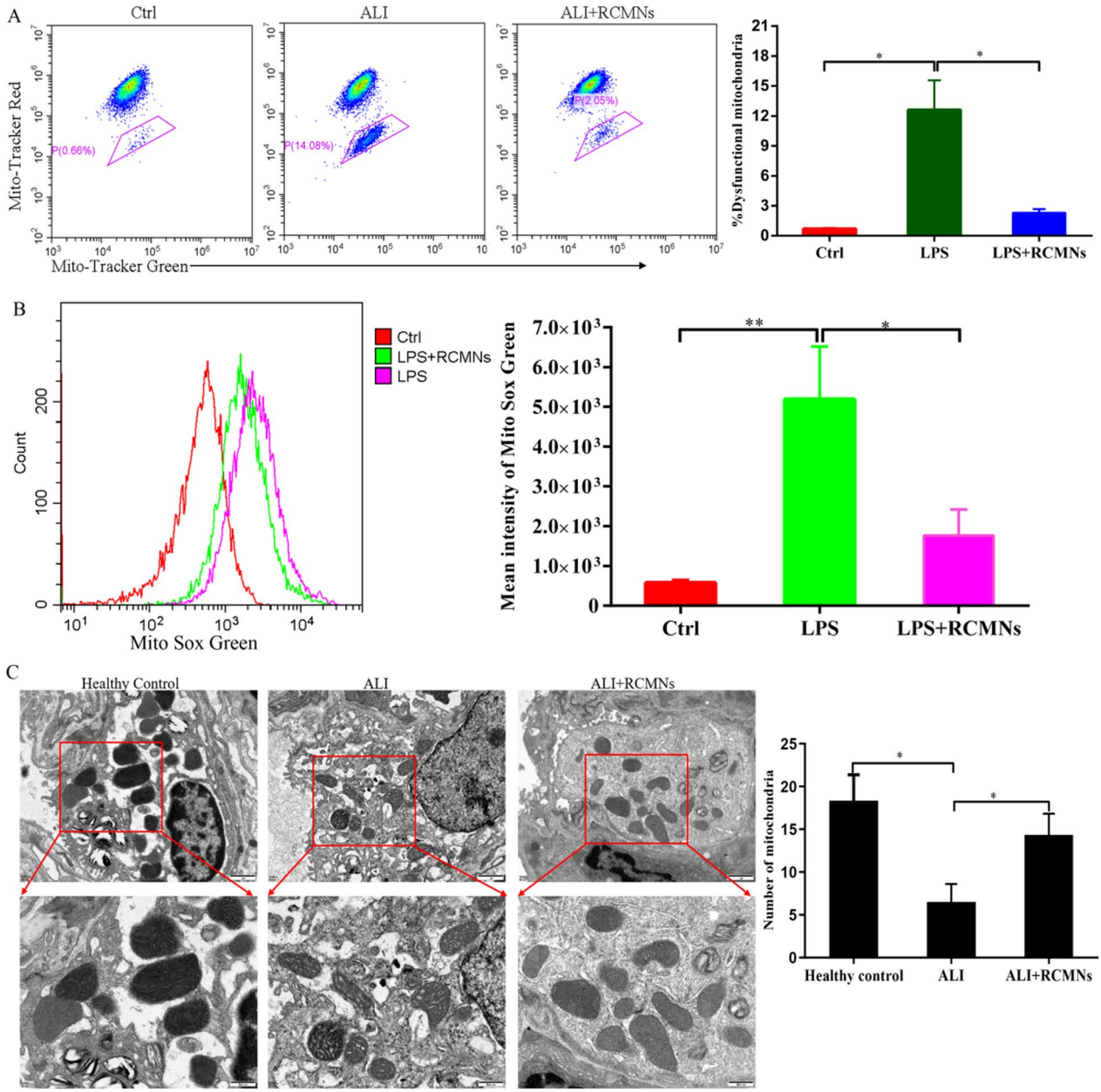

Fig. 4 RCMNs effectively scavenge reactive oxygen species (ROS) in macrophages and improve mitochondrial function. **A** Flow cytometry analysis of mitochondria stained with Mito Tracker Red and Mito Tracker Green ($Green^{+}/Red^{-}$). **B** Quantification of mitochondrial ROS levels by staining with MitoSox and subsequent flow cytometry analysis revealed the effects of RCMNs on mitochondrial function. **C** Representative transmission electron micrographs (TEM) provided visual evidence of mitochondrial amount, morphology, and cristae structure, while the histogram quantified changes in mitochondrial size and number

key biological processes, including mitochondrial respiratory chain complex IV assembly, oxidative phosphorylation, and mitochondrial respiratory chain complex I assembly. These findings suggest that RCMNs exert their therapeutic effects by modulating the expression of genes critical to mitochondrial function and energy metabolism. The Kyoto Encyclopedia of Genes and Genomes (KEGG) pathway analysis has revealed that RCMs primarily exert their biological functions by modulating several key signaling pathways, including the Calcium signaling pathway, TNF signaling pathway, and Toll-like receptor signaling pathway. These findings suggest that RCMs play a crucial role in regulating cellular processes such as calcium homeostasis, inflammation, and

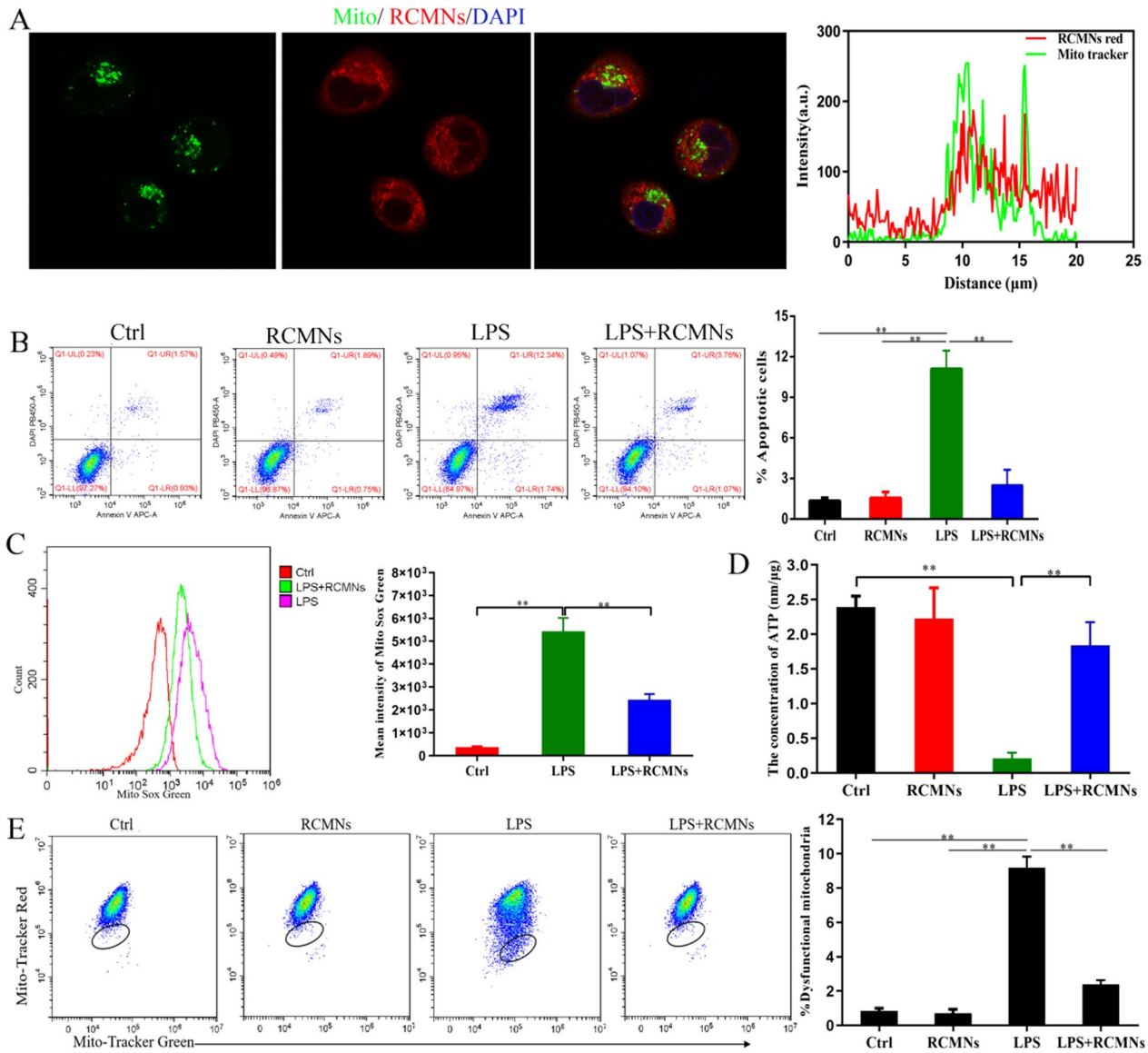

Fig. 5 Targeting capability of RCMNs to pulmonary macrophages. **A** The co-localization of RCMNs and mitochondria in MH-S cells was examined through confocal microscopy, revealing that RCMNs emitted red fluorescence. Meanwhile, the nuclei were distinctly stained blue with Hochest, and the mitochondria appeared green due to staining with Mito Tracker green. The accompanying graph on the right depicts the fluorescence intensity, measured in arbitrary units (AU), on the y-axis, plotted against the distance in nanometers on the x-axis. **B** Detection of the effect of RCMNs on LPS-induced apoptosis in MH-S Cells using Annexin V/PI staining. **C** Quantitative effect of RCMNs on mitochondrial reactive oxygen species (ROS) levels in LPS treated MH-S cells by flow cytometry after MitoSox staining. **D** The effect of RCMNs on ATP levels in LPS treated MH-S cells. **E** Flow cytometric analysis of Mitochondria stained with Mito Tracker Red and Mito Tracker Green, focusing on the Green^{+}/Red^{-} population

immune responses, which are essential for maintaining normal physiological functions and responding to various environmental stimuli and pathological conditions (Fig. 6D). Further analysis of the co-expression network of differentially expressed genes has shown that CCL5, ISG15, CCR2, and CXCL2 play crucial roles in the anti-inflammatory response mediated by RCMNs (Fig. 6E). These genes are differently expressed in response to RCMNs treatment and are closely interconnected within the gene network, suggesting that they work together to regulate inflammatory processes. CCL5 and CCR2 are involved in the recruitment and activation of immune cells, while ISG15 and CXCL2 have been implicated in the modulation of inflammatory signaling and the production of inflammatory mediators. Gene Set Enrichment Analysis (GSEA) results have also confirmed that

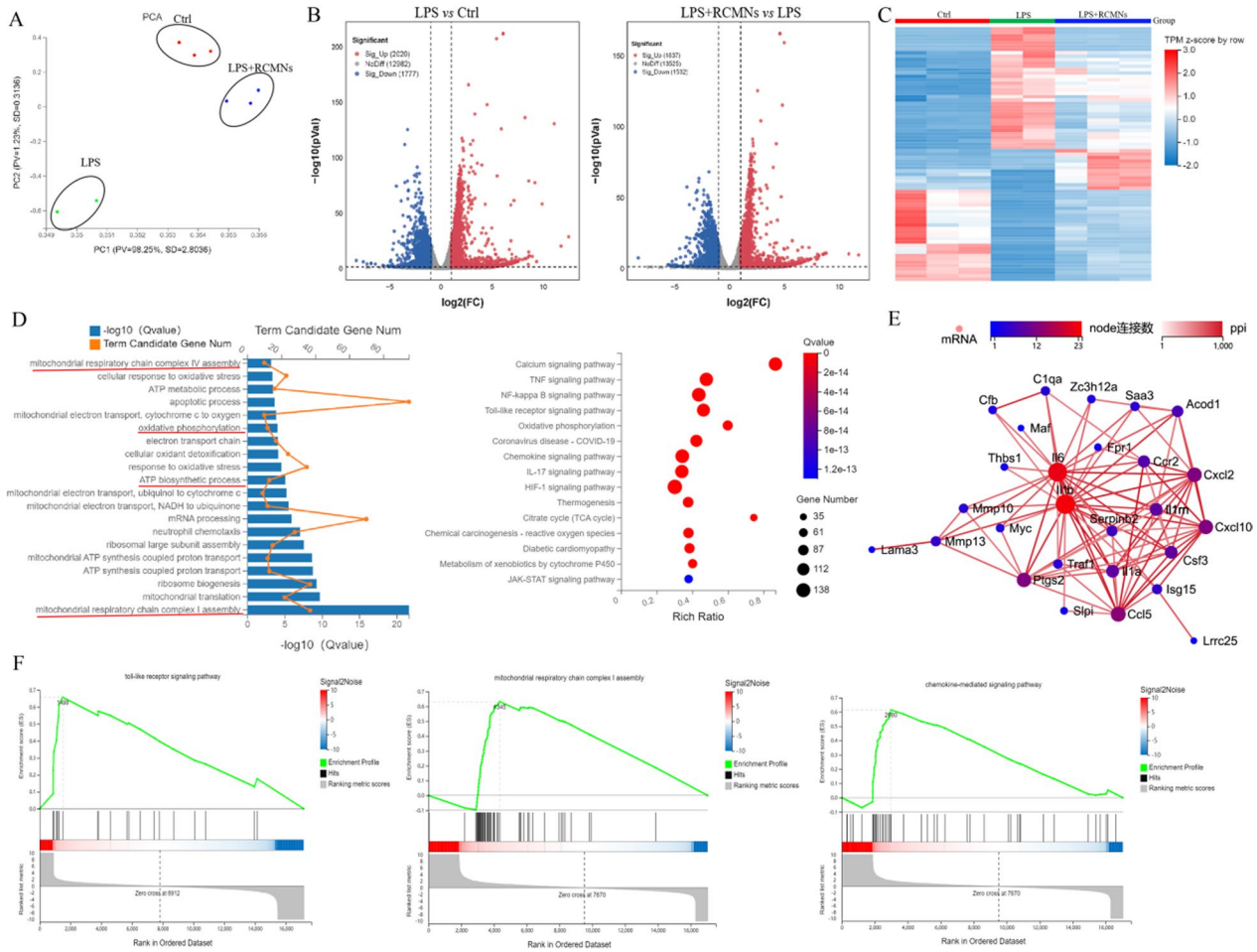

Fig. 6 Identify the mechanism of RCMNs in improving ALI through RNA-seq transcriptome analysis. **A** Principal component analysis (PCA) of the control group, LPS group, and LPS + RCMNs group. **B** Global analysis of differentially expressed genes in Ctrl vs. LPS and LPS vs. LPS + RCMNs (**C**) The heatmap displays the top 80 differentially expressed genes across three study groups: control, LPS, and LPS + RCMNs. **D** Functional enrichment analysis of differential genes and KEGG pathway enrichment analysis. **E** Co-expression network of significantly differential genes after RCMNs treatment in ALI. **F** Significantly different gene enrichment analysis (GSEA) after treating ALI with RCMNs

RCMNs primarily exert their effects in LPS-stimulated MH-S cells through the Toll-like receptor signaling pathway, mitochondrial respiratory chain complex I assembly, and chemokine-mediated signaling pathway. These findings suggest that RCMNs modulate immune responses, mitochondrial function, and chemotactic signaling to exert their therapeutic effects in inflamed cells (Fig. 6F). Together, these findings highlight the multifaceted mechanisms by which RCMNs may exert their protective effects in LPS-induced inflammation.

RCMNs improve LPS-induced macrophage mitochondrial dysfunction by regulating intracellular Ca^{2+} levels

Mitochondria are crucial organelles in cells that are responsible for energy production, cellular metabolism, and apoptosis. However, during acute lung injury (ALI), mitochondrial dysfunction can occur, leading to impaired cellular energetic, increased oxidative stress, and altered calcium homeostasis. Our above experimental results demonstrate that, in the context of acute lung injury, the primary anti-inflammatory mechanism of RCMNs is achieved by specifically targeting the mitochondria of pulmonary macrophages, thereby mitigating their dysfunctional state. To further validate these findings, PCR array for mitochondrial energy metabolism in mice was employed. Notably, the findings revealed elevated expression of mitochondrial gene networks representing respiratory chain complexes I, II, III, IV, and V in with LPS-stimulated MH-S cells treated with RCMNs (Fig. 7A–E). Abnormal Ca^{2+} levels can contribute to the development and severity of acute lung injury, as calcium ions play a crucial role

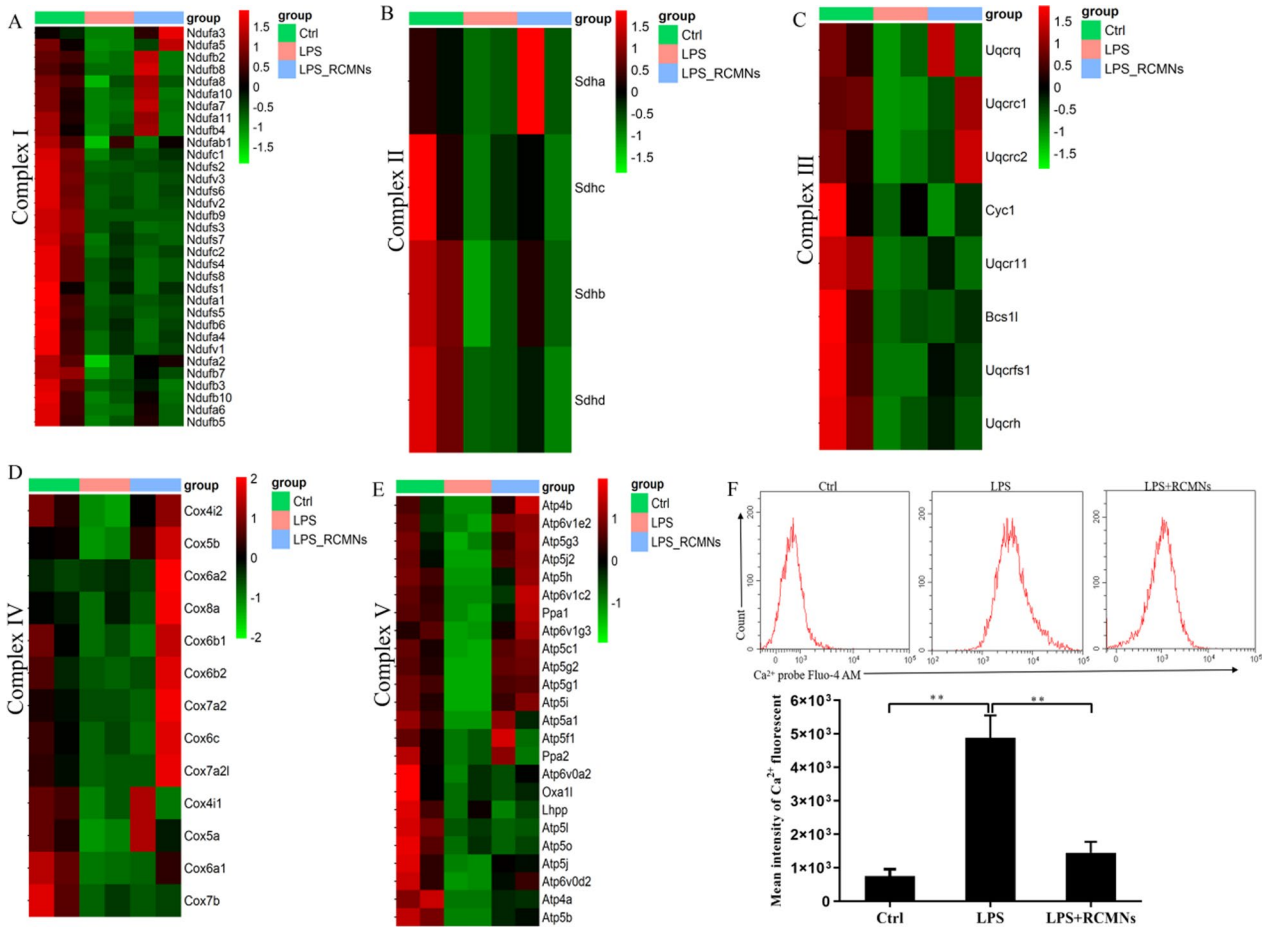

Fig. 7 RCMNs regulate mitochondrial respiratory chain genes and downregulate intracellular Ca^{2+}levels. **A**–**E** Heatmap depicting qPCR-based detection of mitochondrial respiratory chain complex I, II, III, IV, and V associated gene expression in MH-S cells. **F** Flow cytometry determination of Ca^{2+} fluorescence intensity in MH-S cells

in cell signaling and maintaining lung epithelial integrity. Conversely, acute lung injury can disrupt calcium homeostasis, leading to further calcium ion abnormalities that exacerbate lung damage. To investigate whether RCMNs can mediate abnormal Ca^{2+} levels in ALI, we treated MH-S cells with LPS and utilized a Ca^{2+}-related probe fluo-4. Flow cytometry assays demonstrated that the level of Ca^{2+} increased significantly in cells treated with LPS alone, whereas the presence of RCMNs suppressed this LPS-induced Ca^{2+} release, indicating their potential role in down-regulating intracellular Ca^{2+} concentration (Fig. 7F). These results suggest that RCMNs specifically target mitochondria in pulmonary macrophages to mitigate mitochondrial dysfunction during acute lung injury, leading to improved mitochondrial gene networks, respiratory chain complexes expression, and normalized intracellular calcium levels, indicating a potential therapeutic approach to reducing lung damage.

Biocompatibility evaluation of RCMNs in *vivo*

Evaluating the biocompatibility of RCMNs in *vivo* involves assessing their interactions with living tissues and the potential for adverse biological responses. This evaluation typically includes studies on the distribution, clearance, and long-term effects of the RCMNs within the body. The in *vivo* toxicity of RCMNs was assessed at a dose of 10 mg kg^{-1}, with results indicating minimal to no adverse effects on vital organs, including the heart, liver, intestine, lung, kidney and spleen as confirmed through hematoxylin and eosin (H&E) staining imaging(Fig. 8A). Blood routine results for mice in the PBS group, as well as those at 7 days and 30 days post-injection of RCMNs, were all within normal ranges (Fig. 8B). Levels of alanine transaminase (ALT), aspartate transaminase (AST), creatinine (CREA), and blood urea nitrogen (BUN) were

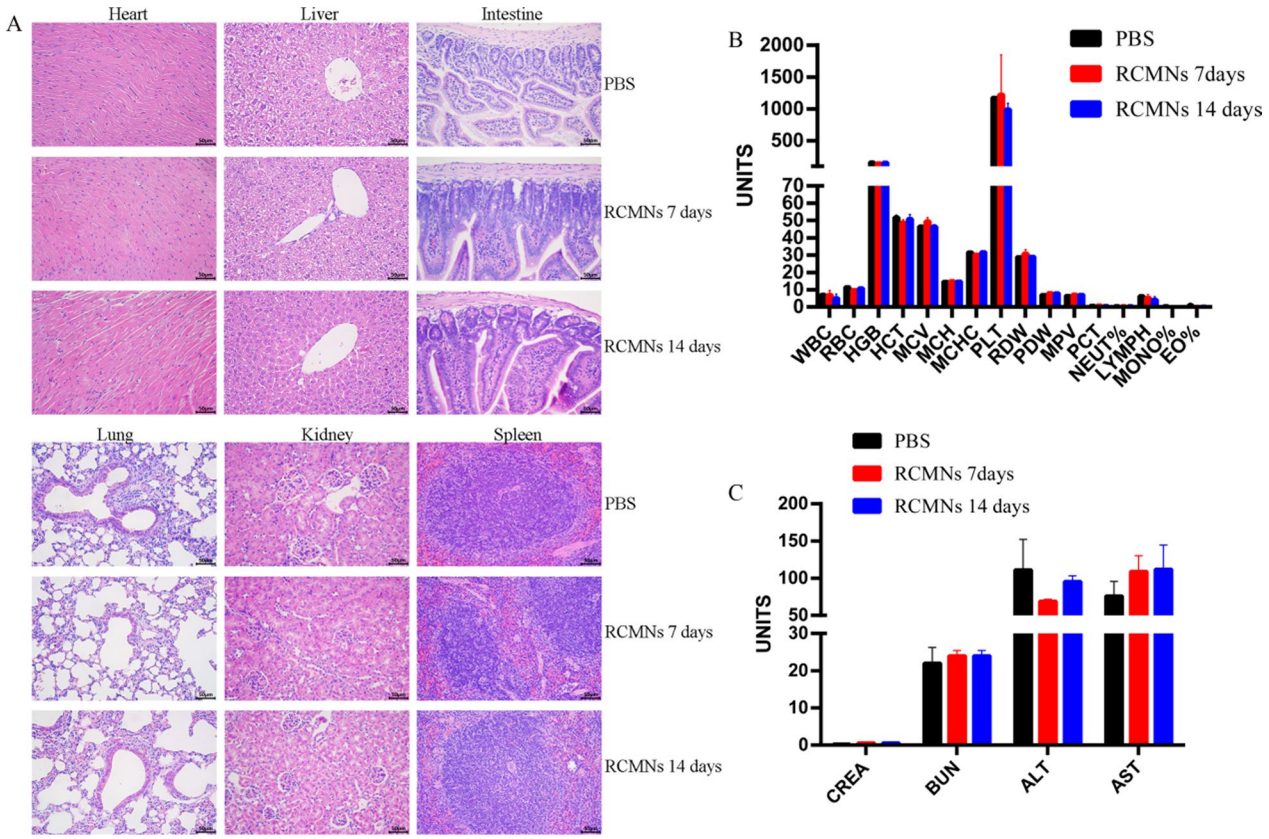

Fig. 8 Toxicity of RCMN in *vivo*. **A** H&E staining of heart, liver, intestine, lung, kidney and spleen after RCMNs treatment at 7 and 30 days.**B** Blood routine data were collected from the PBS injection group, serving as a control, as well as from mice that underwent RCMNs injection at 7 and 30 days. **C** Analysis of serum biochemical indicators from PBS injection group (used as blank control) and mice receiving RCMNs injection at different time points

measured to assess the potential impact of RCMNs on liver and kidney functions. The levels of ALT, AST, ALP, CREA, and BUN in mice at 7 and 30 days post-injection of RCMNs were comparable to those in the PBS group, indicating that RCMNs did not cause any damage to the kidneys or liver of the mice (Fig. 8C). Collectively, these findings suggest that RCMNs are both effective and safe for the treatment of acute lung injury (ALI).

Discussion

Acute Lung Injury (ALI) is a severe lung condition caused by various factors including infections, trauma, and inhalation of harmful substances, marked by lung inflammation leading to impaired gas exchange and breathing difficulties [21–23]. Previous studies have demonstrated a strong correlation between ALI and unregulated Reactive Oxygen Species (ROS). ROS are highly reactive molecules that can damage cells and tissues, leading to inflammation and tissue injury. Therefore, scavenging ROS has been identified as a promising therapeutic strategy for treating ALI [24–27].

In this study, we aimed to develop a novel therapeutic strategy targeting ROS-mediated inflammation in ALI by synthesizing ROS-responsive red fluorescent carbon dot-TK-methylprednisolone nanoparticles (RCMNs). Our findings demonstrate the potential of these nanoparticles as an effective treatment for ALI due to their unique ability to specifically target and scavenge ROS in lung macrophages. One of the primary findings of this study is that RCMNs accumulate specifically in the lungs of ALI mice, as evidenced by in vivo imaging experiments. This observation suggests that RCMNs possess inherent targeting capabilities towards sites of inflammation and ROS-damaged tissue. The specific targeting of lung macrophages, which are the primary immune cells involved in pathogenesis of ALI, further underscores the potential therapeutic benefit of RCMNs. Our results indicate that RCMNs effectively reduce lung damage and inflammation in ALI models. Histological assessment of lung tissue from treated mice revealed reduced inflammatory cell infiltration and thinning of the alveolar wall, indicating alleviation of lung injury. This finding is supported by

the improved survival rate observed in endotoxic shock models, further demonstrating the protective effects of RCMNs.

Nanoparticles exhibit numerous advantages in eliminating ROS during ALI. These particles efficiently scavenge excessive ROS, thereby reducing oxidative stress and inflammation within lung tissue [28–30]. Their diminutive size facilitates precise targeting to specific lung regions, thereby boosting treatment effectiveness. Nanoparticles can be tailored to respond to distinct biological signals, facilitating the controlled release of ROS-scavenging agents for targeted ALI therapy [31–33].

Mechanistically, RCMNs alleviate inflammation in ALI by targeting the dysfunctional mitochondria of macrophages. Dysfunctional mitochondria within these immune cells lead to excessive ROS production, which exacerbates lung tissue damage and inflammatory responses. Our studies demonstrate that RCMNs alleviate mitochondrial ROS stress, reduce dysfunctional mitochondria, and improve mitochondrial morphology in primary macrophages isolated from mice with ALI. These effects were accompanied by improved mitochondrial membrane potential and ATP production, indicating enhanced mitochondrial function. To gain further insights into the molecular mechanisms of RCMNs, we performed RNA-seq transcriptome analysis of LPS-stimulated MH-S cells treated with RCMNs. Functional enrichment analysis revealed that RCMNs modulate genes critical to mitochondrial respiratory chain complex assembly, oxidative phosphorylation, and energy metabolism. This finding is consistent with the observed improvements in mitochondrial function and energy production in macrophages treated with RCMNs. Additionally, RCMNs were found to regulate key signaling pathways involved in inflammation and immune responses, including the Calcium signaling pathway, TNF signaling pathway, and Toll-like receptor signaling pathway.The suppression of LPS-induced calcium ion abnormalities by RCMNs is particularly noteworthy, as abnormal Ca^{2+} levels can contribute to the severity of ALI. In summary, we have developed a nanoparticle RCMNs for scavenging intracellular ROS and synergistically mitigating inflammation during the progression of ALI.

Conclusion

In summary, this study demonstrates the therapeutic potential of ROS-responsive RCMNs in the treatment of acute lung injury (ALI). By specifically targeting dysfunctional mitochondria in lung macrophages, RCMNs effectively scavenge reactive oxygen species (ROS), alleviate inflammation, and enhance mitochondrial function. The regulation of key signaling pathways and intracellular calcium levels by RCMNs further underscores their significance in maintaining normal physiological functions in ALI. Overall, our findings suggest that RCMNs represent a promising therapeutic approach for ALI and warrant further investigation in clinical settings.

Author contributions

Haiyu Li and Fangzhou Song performed the experiment and wrote and drafted the manuscript. Wenna Fan, Yongyao Tang and Yamin Liu performed the material synthesis and validation through in vitro experiments. Ya Ran, Xin Song and Guangrui Pan performed the bioinformatics analysis and animal experiments. Li Mai, Xue Jiang, and Dan Chen retrieved the data and performed the statistical analysis. All authors read and approved the final manuscript.

Funding

This work was supported by the National Natural Science Foundation of China [No.82002154], and the General Project of Chongqing Basic Research and Frontier Exploration Project (Natural Science Foundation), China [No. cstc2019jcyj-msxmX0029].

Availability of data and materials

No datasets were generated or analysed during the current study.

Declarations

Ethics approval and consent to participate

This research protocol has been approved by the Experimental Animal Management and Use Committee of Chongqing Medical University (Approval Number: IACUC-CQMU-2023-0289).

Competing interests

The authors declare no competing interests.

Author details

[1]Institute of Intelligent Chinese Medicine, Chongqing University of Chinese Medicine, Chongqing 402760, China. [2]Molecular Medicine and Cancer Research Center, Chongqing Medical University, Chongqing 400016, China. [3]Department of Obstetrics and Gyecology, Women and Children's Hospital of Chongqing Medical University/Chongqing Health Center for Women and Children, Chongqing 400016, China. [4]General Surgery, Qianjiang Districet Chinese Medicine Hospital, Qianjiang District, Chongqing 409000, China. [5]General Surgery (Breast Surgery), The Affiliated Hospital of Southwest Medical University, 25 Taiping Rd, Jiangyang District, Luzhou 646000, Sichuan, China. [6]Department of Laboratory Medicine, The Second Affiliated Hospital of Chongqing Medical University, Chongqing 400010, China.

Received: 12 July 2024 Accepted: 14 November 2024
Published online: 22 November 2024

References

1. Wang YH, Yan ZZ, Luo SD, Hu JJ, Wu M, Zhao J, Liu WF, Li C, Liu KX. Gut microbiota-derived succinate aggravates acute lung injury after intestinal ischaemia/reperfusion in mice. Euro Resp J. 2023. https://doi.org/10.1183/13993003.00840-2022.
2. Li Y, Cao Y, Xiao J, Shang J, Tan Q, Ping F, Huang W, Wu F, Zhang H, Zhang X. Inhibitor of apoptosis-stimulating protein of p53 inhibits ferroptosis and alleviates intestinal ischemia/reperfusion-induced acute lung injury. Cell Death Differ. 2020;27:2635–50.
3. Herold S, Becker C, Ridge KM, Budinger GR. Influenza virus-induced lung injury: pathogenesis and implications for treatment. Eur Respir J. 2015;45:1463–78.
4. Yamashita M, Niisato M, Kawasaki Y, Karaman S, Robciuc MR, Shibata Y, Ishida Y, Nishio R, Masuda T, Sugai T, Ono M, Tuder RM, Alitalo K, Yamauchi

K. VEGF-C/VEGFR-3 signalling in macrophages ameliorates acute lung injury. Euro Resp J. 2022. https://doi.org/10.1183/13993003.00880-2021.
5. Clementi N, Ghosh S, De Santis M, Castelli M, Criscuolo E, Zanoni I, Clementi M, Mancini N. Viral respiratory pathogens and lung injury. Clin Microbiol Rev. 2021. https://doi.org/10.1128/CMR.00103-20.
6. Xia L, Zhang C, Lv N, Liang Z, Ma T, Cheng H, Xia Y, Shi L. AdMSC-derived exosomes alleviate acute lung injury via transferring mitochondrial component to improve homeostasis of alveolar macrophages. Theranostics. 2022;12:2928–47.
7. Guo Y, Liu Y, Zhao S, Xu W, Li Y, Zhao P, Wang D, Cheng H, Ke Y, Zhang X. Oxidative stress-induced FABP5 S-glutathionylation protects against acute lung injury by suppressing inflammation in macrophages. Nat Commun. 2021;12:7094.
8. Park I, Kim M, Choe K, Song E, Seo H, Hwang Y, Ahn J, Lee SH, Lee JH, Jo YH, Kim K, Koh GY, Kim P. Neutrophils disturb pulmonary microcirculation in sepsis-induced acute lung injury. The Euro Resp J. 2019. https://doi.org/10.1183/13993003.00786-2018.
9. Yuan R, Li Y, Han S, Chen X, Chen J, He J, Gao H, Yang Y, Yang S, Yang Y. Fe-Curcumin nanozyme-mediated reactive oxygen species scavenging and anti-inflammation for acute lung injury. ACS Cent Sci. 2022;8:10–21.
10. Long G, Gong R, Wang Q, Zhang D, Huang C. Role of released mitochondrial DNA in acute lung injury. Front Immunol. 2022;13: 973089.
11. Morrison T, Jackson M, Cunningham E, Kissenpfennig A, McAuley D, O'Kane C, Krasnodembskaya A. Mesenchymal stromal cells modulate macrophages in clinically relevant lung injury models by extracellular vesicle mitochondrial transfer. Am J Respir Crit Care Med. 2017;196:1275–86.
12. Huang W, Wen L, Tian H, Jiang J, Liu M, Ye Y, Gao J, Zhang R, Wang F, Li H, Shen L, Peng F, Tu Y. Self-propelled proteomotors with active cell-free mtDNA clearance for enhanced therapy of sepsis-associated acute lung injury. Adv Sci. 2023;10: e2301635.
13. Zmijewski J, Lorne E, Zhao X, Tsuruta Y, Sha Y, Liu G, Siegal G, Abraham E. Mitochondrial respiratory complex I regulates neutrophil activation and severity of lung injury. Am J Respir Crit Care Med. 2008;178:168–79.
14. Yan J, Tang Z, Li Y, Wang H, Hsu J, Shi M, Fu Z, Ji X, Cai W, Ni D, Qu J. Molybdenum nanodots for acute lung injury therapy. ACS Nano. 2023;17:23872–88.
15. Wang K, Rong G, Gao Y, Wang M, Sun J, Sun H, Liao X, Wang Y, Li Q, Gao W, Cheng Y. Fluorous-tagged peptide nanoparticles ameliorate acute lung injury via lysosomal stabilization and inflammation inhibition in pulmonary macrophages. Small. 2022;18: e2203432.
16. Chabot F, Mitchell J, Gutteridge J, Evans T. Reactive oxygen species in acute lung injury. Eur Respir J. 1998;11:745–57.
17. Chen G, Song X, Wang B, You G, Zhao J, Xia S, Zhang Y, Zhao L, Zhou H. Carboxyfullerene nanoparticles alleviate acute hepatic injury in severe hemorrhagic shock. Biomaterials. 2017;112:72–81.
18. Seeley E, Rosenberg P, Matthay M. Calcium flux and endothelial dysfunction during acute lung injury: a STIMulating target for therapy. J Clin Investig. 2013;123:1015–8.
19. Ji H, Zhang C, Xu F, Mao Q, Xia R, Chen M, Wang W, Lv S, Li W, Shi X. Inhaled pro-efferocytic nanozymes promote resolution of acute lung injury. Adv Sci. 2022;9: e2201696.
20. Imai Y, Kuba K, Neely G, Yaghubian-Malhami R, Perkmann T, van Loo G, Ermolaeva M, Veldhuizen R, Leung Y, Wang H, Liu H, Sun Y, Pasparakis M, Kopf M, Mech C, Bavari S, Peiris J, Slutsky A, Akira S, Hultqvist M, Holmdahl R, Nicholls J, Jiang C, Binder C, Penninger J. Identification of oxidative stress and Toll-like receptor 4 signaling as a key pathway of acute lung injury. Cell. 2008;133:235–49.
21. Bos L, Ware L. Acute respiratory distress syndrome: causes, pathophysiology, and phenotypes. Lancet. 2022;400:1145–56.
22. Brower R, Matthay M, Morris A, Schoenfeld D, Thompson B, Wheeler A. Ventilation with lower tidal volumes as compared with traditional tidal volumes for acute lung injury and the acute respiratory distress syndrome. N Engl J Med. 2000;342:1301–8.
23. Fan E, Brodie D, Slutsky A. Acute respiratory distress syndrome: advances in diagnosis and treatment. JAMA. 2018;319:698–710.
24. Wendisch D, Dietrich O, Mari T, von Stillfried S, Ibarra I, Mittermaier M, Mache C, Chua R, Knoll R, Timm S, Brumhard S, Krammer T, Zauber H, Hiller A, Pascual-Reguant A, Mothes R, Bülow R, Schulze J, Leipold A, Djudjaj S, Erhard F, Geffers R, Pott F, Kazmierski J, Radke J, Pergantis P, Baßler K, Conrad C, Aschenbrenner A, Sawitzki B, Landthaler M, Wyler E, Horst D, Hippenstiel S, Hocke A, Heppner F, Uhrig A, Garcia C, Machleidt F, Herold S, Elezkurtaj S, Thibeault C, Witzenrath M, Cochain C, Suttorp N, Drosten C, Goffinet C, Kurth F, Schultze J, Radbruch H, Ochs M, Eils R, Müller-Redetzky H, Hauser A, Luecken M, Theis F, Conrad C, Wolff T, Boor P, Selbach M, Saliba A, Sander L. SARS-CoV-2 infection triggers profibrotic macrophage responses and lung fibrosis. Cell. 2021;184:6243-6261.e6227.
25. Wiedemann H, Wheeler A, Bernard G, Thompson B, Hayden D, deBoisblanc B, Connors A, Hite R, Harabin A. Comparison of two fluid-management strategies in acute lung injury. New England J Med. 2006;354:2564–75.
26. Clementi N, Ghosh S, De Santis M, Castelli M, Criscuolo E, Zanoni I, Clementi M, Mancini N. Viral respiratory pathogens and lung injury. Clin Microbiol Rev. 2021;34(3):10–28.
27. Mirchandani A, Jenkins S, Bain C, Sanchez-Garcia M, Lawson H, Coelho P, Murphy F, Griffith D, Zhang A, Morrison T, Ly T, Arienti S, Sadiku P, Watts E, Dickinson R, Reyes L, Cooper G, Clark S, Lewis D, Kelly V, Spanos C, Musgrave K, Delaney L, Harper I, Scott J, Parkinson N, Rostron A, Baillie J, Clohisey S, Pridans C, Campana L, Lewis P, Simpson A, Dockrell D, Schwarze J, Hirani N, Ratcliffe P, Pugh C, Kranc K, Forbes S, Whyte M, Walmsley S. Hypoxia shapes the immune landscape in lung injury and promotes the persistence of inflammation. Nat Immunol. 2022;23:927–39.
28. Salazar-Puerta A, Rincon-Benavides M, Cuellar-Gaviria T, Aldana J, Vasquez Martinez G, Ortega-Pineda L, Das D, Dodd D, Spencer C, Deng B, McComb D, Englert J, Ghadiali S, Zepeda-Orozco D, Wold L, Gallego-Perez D, Higuita-Castro N. Engineered extracellular vesicles derived from dermal fibroblasts attenuate inflammation in a murine model of acute lung injury. Adv Mater. 2023;35: e2210579.
29. Li D, Zhao A, Zhu J, Wang C, Shen J, Zheng Z, Pan F, Liu Z, Chen Q, Yang Y. Inhaled lipid nanoparticles alleviate established pulmonary fibrosis. Small. 2023;19: e2300545.
30. Chen K, Zhang Z, Fang Z, Zhang J, Liu Q, Dong W, Liu Y, Wang Y, Wang J. Aged-signal-eliciting nanoparticles stimulated macrophage-mediated programmed removal of inflammatory neutrophils. ACS Nano. 2023;17:13903–16.
31. Fei Q, Shalosky E, Barnes R, Shukla V, Xu S, Ballinger M, Farkas L, Lee R, Ghadiali S, Englert J. Macrophage-targeted lipid nanoparticle delivery of microRNA-146a to mitigate hemorrhagic shock-induced acute respiratory distress syndrome. ACS Nano. 2023;17:16539–52.
32. Dahmer M, Yang G, Zhang M, Quasney M, Sapru A, Weeks H, Sinha P, Curley M, Delucchi K, Calfee C, Flori H. Identification of phenotypes in paediatric patients with acute respiratory distress syndrome: a latent class analysis, the lancet. Respir Med. 2022;10:289–97.
33. Madl A, Plummer L, Carosino C, Pinkerton K. Nanoparticles, lung injury, and the role of oxidant stress. Annu Rev Physiol. 2014;76:447–65.

Publisher's Note